Journal of Magnetic Resonance 203 (2010) 323–327

Contents lists available at ScienceDirect

Journal of Magnetic Resonance

journal homepage: www.elsevier.com/locate/jmr

Communication

New high dielectric constant materials for tailoring the B_1^+ distribution at high magnetic fields

K. Haines [a], N.B. Smith [b,c], A.G. Webb [c,*]

[a] Department of Electrical Engineering, Pennsylvania State University, University Park, PA, USA
[b] Department of Bioengineering, Pennsylvania State University, University Park, PA, USA
[c] C.J.Gorter Center for High Field MRI, Leiden University Medical Center, Leiden, The Netherlands

ARTICLE INFO

Article history:
Received 19 November 2009
Revised 6 January 2010
Available online 11 January 2010

Keywords:
Dielectric materials
High-field MRI
Transmit arrays
Electromagnetics

ABSTRACT

The spatial distribution of electromagnetic fields within the human body can be tailored using external dielectric materials. Here, we introduce a new material with high dielectric constant, and also low background MRI signal. The material is based upon metal titanates, which can be made into a geometrically-formable suspension in de-ionized water. The material properties of the suspension are characterized from 100 to 400 MHz. Results obtained at 7 T show a significant increase in image intensity in areas such as the temporal lobe and base of the brain with the new material placed around the head, and improved performance compared to purely water-based gels.

1. Introduction

Sample-induced inhomogeneities in the distribution of electromagnetic (EM) energy for human MRI at high magnetic fields are well documented [1–7]. These inhomogeneities arise primarily from the dielectric properties of tissue, which result in partial constructive and destructive RF interactions from complex wave behavior. The effective wavelength of EM energy in tissue is ~13 cm for white and gray matter at 7 T and ~11 cm at 9.4 T. The brain has dimensions similar to, and the abdomen dimensions considerably larger than, the EM wavelength at these field strengths. Standard volume resonators geometries, such as the birdcage [8] and the transverse electromagnetic mode (TEM) [9], which produce homogeneous transmit and receive fields at low magnetic fields, cannot produce the same homogeneous fields as the static magnetic field increases [1,2]. These geometries are designed such that the current elements on opposite sides of the resonator are equal in magnitude but opposite in phase. If the sample within the resonator is greater than a wavelength, areas of destructive interference occur. Manipulating the geometric distribution of EM fields within the human body has a long history of both theoretical and experimental development, driven initially by the field of therapeutic hyperthermia [10–13]. Using an approach derived from such developments, one solution to at least partially solving the inhomogeneous EM distribution for high-field MRI is to drive each element of a resonator separately with a variable magnitude and phase, the so-called transmit-array approach [2,14–18]. Other approaches involve the design of specialized radiofrequency (RF) pulses [19,20], or the combination of these two approaches of RF pulse design and transmit arrays [21–25].

An alternative, though ultimately also complementary, and very simple approach to "directing" the transmit RF field has been demonstrated by Yang et al. [26] at 7 T using water bags placed around the head. The use of pads with high dielectric constant has also been demonstrated at 3 T and is in common clinical practice at many institutions for routine body imaging at 3 T. For example, Sreenivas et al. [27] used 4-L bags filled with water, doped with between 20 and 50 mM manganese salts. Similar work has been reported in phantoms by Takayama et al. [28] and Sunaga et al. [29], who designed a gel with dielectric constant similar to tissue for improved impedance matching to human skin. The basic mechanism by which the RF spatial distribution can be altered using such external high-dielectric structures, summarized by Yang et al. [26], follows from one of Maxwell's equations:

$$\nabla \times \boldsymbol{H} = \boldsymbol{J}_c + \boldsymbol{J}_D = \sigma \boldsymbol{E} + i\varepsilon_r \varepsilon_0 \omega \boldsymbol{E} \quad (1)$$

where $\boldsymbol{H}$ is the magnetic field, $\boldsymbol{J}_c$ the conductive current, $\boldsymbol{J}_D$ the displacement current, σ the conductivity, $\boldsymbol{E}$ the electric field, ε_r the relative dielectric constant of the material and ε_0 that of vacuum. The inclusion of an external high-dielectric material results in high displacement currents within this material, which in turn produces a separate RF field, in addition to that of the RF coil, close to the material.

* Corresponding author. Address: C.J.Gorter Center for High Field MRI, Department of Radiology, C3-Q, Leiden University Medical Center, Albinusdreef 2, Leiden 2333 ZA, The Netherlands. Fax: +31 71 524 8256.
E-mail address: a.webb@lumc.nl (A.G. Webb).

1090-7807/$ - see front matter © 2010 Elsevier Inc. All rights reserved.
doi:10.1016/j.jmr.2010.01.003

Pads in current use have a relative dielectric constant of ~60, and since they contain significant paramagnetic concentrations, can cause significant signal loss in adjacent tissue in single-shot or long echo-time gradient-echo sequences due to strong magnetic susceptibility effects. Particularly for studies at high magnetic fields, one would ideally like a material which has a dielectric constant higher than water (but which also offers the possibility to be tailored in value), a low background signal without paramagnetic doping, and one which can be geometrically formed in order to adapt to different patient sizes.

With respect to obtaining higher dielectric constants, our group has recently designed RF coils for microimaging studies at 600 MHz using ceramic dielectric resonators [30,31]. These resonators are constructed from high-temperature-sintered and cold-pressed samples of barium strontium titanate ($Ba_{0.04}$ $Sr_{0.96}$ TiO_3) [31], which has a very high relative permittivity of 323, and calcium titanate [30], which has a relative permittivity of 156. Although these materials have a very high dielectric constant when they are sintered and pressed, the values for the native powders are much lower, since the volume ratio of the powder is only ~40%, i.e., 60% of the volume of a given sample is air, which has a very low dielectric constant. However, by creating a suspension of the powders with de-ionized water, the dielectric constant can be increased, with a value that can be tailored by the appropriate composition of the suspension. Initially, we have concentrated on the use of calcium titanate due to its wide availability and low cost. The properties of these suspensions, as expanded in later sections, are: (i) a high dielectric constant between 100 and 120, (ii) a low background signal due primarily to short T_2 and T_2^* values, but also to a reduced water content, and (iii) a geometrically deformable but stable suspension.

2. Materials and methods

2.1. Material characterization

Calcium titanate ($CaTiO_3$) (Alfa Aesar, Ward Hill, MA), specified $\varepsilon_r = 156$ when sintered, is available as a fine powder with a density of 4.1 g/cc. $CaTiO_3$ was mixed with distilled, de-ionized water in volume/volume ratios up to 40%, at which point the suspension becomes saturated. The dielectric constants and loss tangents were measured as a function of frequency between 100 and 400 MHz using a dielectric probe kit (85070E, Agilent Technologies, Santa Clara, CA) and S_{11} measurements on a network analyzer. The suspension was packed into a plastic bag with dimensions $18 \times 18 \times 2$ cm. For comparison, an identically sized bag was filled with ultrasonic gel (Aquason).

2.2. Magnetic resonance

All MRI experiments were performed on a Philips Achieva whole body 7 T system. The transmit head coil (NM-008A-7P, Nova Medical, Wilmington, MA) is an actively-detunable quadrature birdcage, with 16 elements (each 2.5 cm wide), inside diameter 29.2 cm, outside diameter 37.5 cm, and physical length 26 cm. The B_1 field homogeneity is defined as 15% over a 16 cm^3 diameter of spherical volume (DSV), with superior–inferior coverage of 16 cm. The 16-channel receive phased array (NMSC025-16-7P, Nova Medical, Wilmington, MA) consists of eight radially gapped rows of z-overlapped coil pairs, with inner diameter 25.5 cm. Images to show the basic performance of the new material were acquired with short TR, short TE, low tip angle gradient-echo sequences. High resolution susceptibility-weighted scans were based on image acquisition parameters described in [32]: a gradient-echo sequence with flow compensation, TR/TE/flip angle 750/25 ms/45°, $0.25 \times 0.25 \times 1$ mm spatial resolution, and 22 slices.

The relaxation time values for the dielectric material were estimated by placing the bag in the center of the head coil to ensure a homogeneous B_1 field throughout the sample. T_1-measurement used an inversion-recovery turbo gradient-echo sequence with centric phase encoding: the inversion time was varied to find the value which minimized the signal intensity. T_2-measurements used a series of spin–echo images, each with a different TE value. T_2^* values were estimated using a variable echo-time gradient-echo sequence.

3. Results

3.1. Material characterization

Fig. 1(a) and (b) shows measured values of the relative dielectric constant (real and imaginary components) and loss tangent, as a function of frequency, for different volume fractions of $CaTiO_3$. The dielectric constant is complex, and is given by:

$$\varepsilon_{eff} = \varepsilon'_{eff} - j\varepsilon''_{eff} \tag{2}$$

The loss tangent ($\tan\delta$) is defined as:

$$\tan\delta = \frac{\omega\varepsilon''_{eff} + \sigma}{\omega\varepsilon'} \tag{3}$$

As can be seen from Fig. 1, for pure water the real component of the dielectric constant does not vary with frequency, and the imaginary component is much smaller than the real one. The imaginary component, and therefore also the loss tangent, increases with frequency. This behavior is well known, and has been described in detail in the context of very high field (>20 T) superconducting high-resolution NMR probe design [33]. As the percentage of $CaTiO_3$ increases the real and imaginary components of the dielectric constant increase. Above 150 MHz the real component is essentially frequency independent, whereas the imaginary component decreases with frequency.

As discussed by Sihvola [34], in assigning a single effective dielectric constant to a mixture of two different materials, one assumes that the mixture responds to EM energy as if it were homogeneous. In practice what this means is that the size of any inclusion in the mixture does not exceed one-tenth of the wavelength in the effective medium. In this regime, which is easily met by a suspension of very small $CaTiO_3$ particles in water, theoretical values of dielectric constant as a function of the volume fraction of $CaTiO_3$ can be calculated using simple mixing rules, which can be derived using static or quasi-static assumptions. There are a large number of mixing rules [34], but for this particular case the most appropriate is Lichtenecker's logarithmic power law:

$$\varepsilon_{eff} = \varepsilon_{CaTiO_3}^{f(CaTiO_3)} * \varepsilon_{H_2O}^{(1-f(CaTiO_3))} \tag{4}$$

Fig. 2 shows the results of fitting Eq. (4) to the measured data. It should be noted that the data points corresponding to 10% and 15% $CaTiO_3$ do not fit the power law particularly well due to the physical difficulty of producing a stable suspension at such low volume concentrations: the probe measurements are made at the top of the suspension, so this means that the measured values are underestimates.

Using the sequences outlined in Section 2, the T_1 value for the dielectric pad was measured to be 110 ms, the T_2 value 12 ms, and the T_2^* value less than 2 ms. The shortening of the transverse relaxation times in a suspension is very familiar from the field of porous media magnetic resonance. Fig. 3 shows the results of the first imaging experiments using the new dielectric material. The bag was placed on one side of the volunteer's head, and a low tip angle three-dimensional gradient-echo image acquired with whole-brain coverage. Fig. 3(a) shows a coronal slice through the temporal lobe region. Even with a very short echo time, the signal

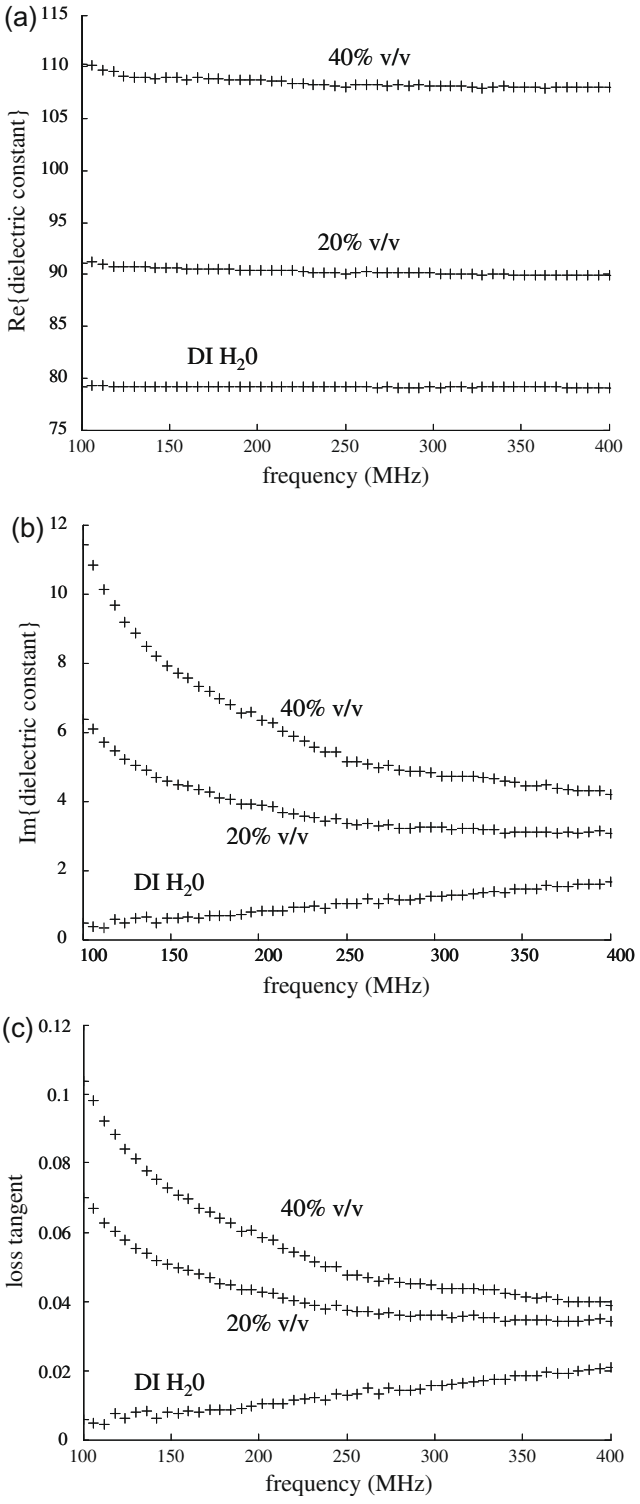

Fig. 1. The real (a) and imaginary (b) relative dielectric constant of different ratios of calcium titanium oxide and de-ionized water as a function of frequency. (c) Corresponding values of the loss tangent.

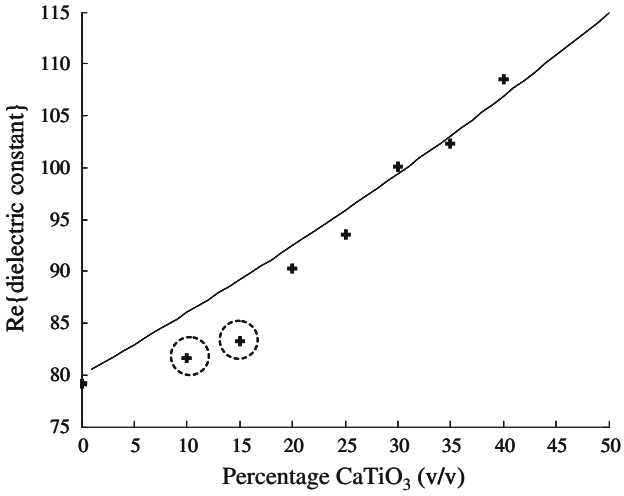

Fig. 2. Plot of the real component of the dielectric constant vs. the volume fraction of $CaTiO_3$ in de-ionized H_2O. The dotted line represents Lichtenecker's logarithmic power law, with the crosses being measured data points. The two circled data points are underestimates due to the difficulty in obtaining a stable suspension for the duration of the measurements.

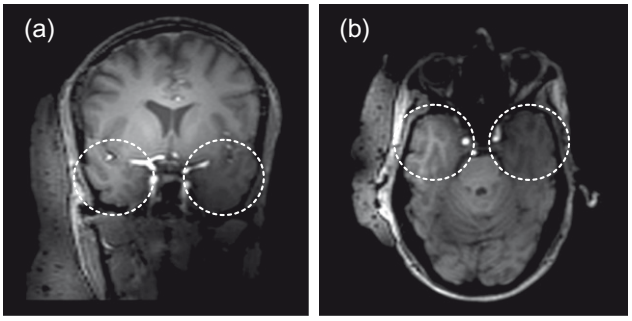

Fig. 3. (a) Coronal and (b) axial low-resolution gradient-echo scans with the dielectric material on one side of the head, TR/TE/FA 4.6/2.2 ms/5°, $1.5 \times 1.5 \times 2$ mm. Targeted areas within the white circles show significant increases (between 70% and 140%) in signal-to-noise ratio.

from the dielectric bag is below that of the brain tissue. This removes many of the problems associated with pure water or gel-bags. These include using a lower than optimal receiver gain (causing dynamic range issues), and difficulties with the automatic resonance frequency determination and shimming routines used on most clinical scanners. Very evident is a significant difference between the areas close to the dielectric materials, and the areas on the contralateral side of the brain (images without the dielectric bag are highly symmetric in terms of showing signal losses on both sides of the brain). The difference in image contrast between gray matter (GM) and white matter (WM) is indicative of a large difference in the strength of the RF transmit field. The higher the B_1 field, the greater the GM/WM contrast due to different T_1 values: a very low tip angle will effectively result in a proton-density-weighted image with very little contrast since the proton-density for GM and WM is very similar. The difference in signal intensities from the two areas in Fig. 3(a) comes from the effects of both transmission and reception. Fig. 3(b) shows the same dataset, reformatted into an axial plane. Signal increases of between 70% and 140% were measured for different regions of the temporal lobe.

In order to compare results between a standard gel and the new dielectric material, equally sized bags were placed on the left and right side of a volunteer's head. A series of axial scans were acquired, again encompassing the temporal lobe region. Fig. 4 shows the images, which show not only a higher signal intensity from the area closest to the new dielectric material, but also the much lower background signal from the material compared to the standard gel bag.

One of the main applications of high-field neuroimaging is the characterization of neurodegenerative diseases such as Alzheimers, Parkinsons, and multiple sclerosis [35,36]. In addition to the improved spatial resolution possible at high field, the use of long

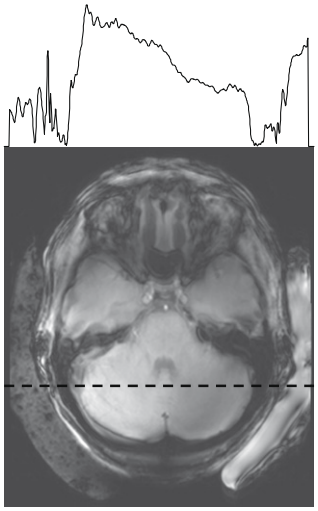

Fig. 4. An axial slice taken just above the level of the temporal lobe. A bag containing the 40% $CaTiO_3$ suspension is placed on the left of the head, with a water bag on the right. A signal projection taken at the level of the dotted line is shown above the image. The image shows a greater signal from the area closer to the $CaTiO_3$ bag, and also a reduced background signal compared to the water bag. Image acquisition parameters: gradient-echo sequence, TR/TE/nominal flip angle 12 ms/ 5 ms/ 15°, 220 × 220 data matrix, 1 × 1 mm in-plane spatial resolution, 3 mm slice thickness.

echo-time susceptibility-weighted and phase imaging [32,37] produces images with very high contrast, particularly in areas of diffuse iron deposition which are associated with many such diseases. Fig. 5 shows an example of this type of very high resolution susceptibility-weighted image acquired from a volunteer using a 40% v/v $CaTiO_3$ bag on one side of the head. The signal from the dielectric bag is effectively in the noise level. Again, there is a significant increase in image quality in the area of the brain close to the bag: there is a much lower image contrast in the contralateral side.

4. Discussion and conclusions

We have characterized a new high-dielectric material using calcium titanium oxide which allows tailoring of the RF spatial distribution at high field. In the head, the high dielectric constant is particularly effective at improving image quality in areas, such as the temporal lobe, usually associated with low signal intensity. In addition to the high dielectric constant, the new material produces a very low background signal intensity, without the need for paramagnetic doping. The 40% volume fraction of dielectric material produces a stable suspension (over many months at least) which can easily be formed to fit around the patient's head within a commercial head coil. All of the images shown in this paper have been single-pulse gradient-echo, since these form the vast majority of our current clinical protocols. However, the beneficial effects of using the new dielectric material would, of course, be much higher in spin–echo sequences as outlined in the article by Yang et al. [26]. A number of new applications and future developments can be considered. Localized spectroscopy in the temporal lobe is potentially very useful in the study of neurodegenerative diseases, since this is an area which is known to be involved in the early stages of plaque development. Pulse sequences for acquiring such spectra involve at least three slice selective RF pulses for localization, either three 90° pulses for stimulated echo acquisition mode (STEAM) or one 90° and two 180° pulses for point resolved spectroscopy (PRESS). Since these RF pulses are slice selective, adiabatic pulses cannot be used, and so the signal-to-noise is highly dependent on having a strong B_1 field. As a result, localized spectroscopy in such areas is very challenging, and to our knowledge has not been routinely implemented at high fields. Based on the results shown here, we anticipate a significant increase in sensitivity by using a suitable geometry of the new dielectric material placed next to the head. In addition, a number of extra RF pulses are used for water suppression, and the quality of water suppression should be improved by having a stronger, more homogeneous B_1 field.

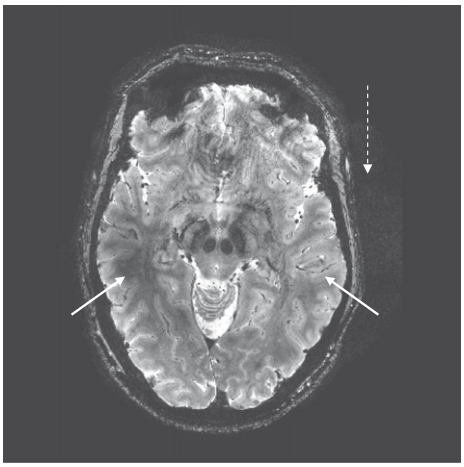

Fig. 5. High resolution susceptibility-weighted scan, showing the signal from the dielectric bag (dotted line and arrow) at noise level. The solid arrows show the increase in B_1 field (right solid arrow) compared to the contralateral side (left solid arrow). TR/TE/FA 750/25 ms/45°, 0.2 5 × 0.25 × 1 mm, 22 slices.

The incorporation of powdered materials with even higher dielectric constant may well enhance these effects yet further. For example, as outlined earlier, $BaSrTiO_3$ ($Ba_{0.04}$ $Sr_{0.96}$ TiO_3) has a relative dielectric constant of 323, and has been used successfully to construct microimaging resonators [31]. However, it is to be anticipated that if the dielectric constant becomes too high, or the geometry/size of the bags is close to a resonant situation [31] then a significant B_1 field may be stored within the dielectric material itself. Given the ability to tune the dielectric constant by simple variation in the composition of the suspensions, and in analogy to impedance matching in microwave and optical applications, the optimum RF distribution may well be achieved by using different layers of materials with different dielectric constants.

Finally, it should be stressed that this approach can be viewed as complementary to other methods, such as the use of transmit arrays, which have already shown extremely high promise for whole body applications at 7 T and above [2,14,16,18]. However, all published images still show significant image non-uniformities. The combination of such transmit arrays with high-dielectric materials adds yet another degree of freedom with which they tackle this challenging problem.

Acknowledgment

The authors thank Dr. Michael Lanagan at Penn State University's Materials Research Institute for valuable advice on dielectric measurements and mixing rules.

References

[1] C.M. Collins, W. Liu, W. Schreiber, Q.X. Yang, M.B. Smith, Central brightening due to constructive interference with, without, and despite dielectric resonance, J. Magn. Reson. Imaging 21 (2005) 192–196.
[2] P.F. van de Moortele, C. Akgun, G. Adriany, S. Moeller, J. Ritter, C.M. Collins, M.B. Smith, J.T. Vaughan, K. Ugurbil, B_1 destructive interferences and spatial phase patterns at 7 T with a head transceiver array coil, Magn. Reson. Med. 54 (2005) 1503–1518.

[3] Q.X. Yang, J. Wang, X. Zhang, C.M. Collins, M.B. Smith, H. Liu, X.H. Zhu, J.T. Vaughan, K. Ugurbil, W. Chen, Analysis of wave behavior in lossy dielectric samples at high field, Magn. Reson. Med. 47 (2002) 982–989.
[4] T.S. Ibrahim, C. Mitchell, P. Schmalbrock, R. Lee, D.W. Chakeres, Electromagnetic perspective on the operation of RF coils at 1.5–11.7 Tesla, Magn. Reson. Med. 54 (2005) 683–690.
[5] A. Kangarlu, B.A. Baertlein, R. Lee, T.S. Ibrahim, L.N. Yang, A.M. Abduljalil, E.M.L. Robitaille, Dielectric resonance phenomena in ultra high field MRI, J. Comput. Assist. Tomogr. 23 (1999) 821–831.
[6] J. Tropp, Image brightening in samples of high dielectric constant, J. Magn. Reson. 167 (2004) 12–24.
[7] T.S. Ibrahim, Y.K. Hue, L. Tang, Understanding and manipulating the RF fields at high field MRI, NMR Biomed. 22 (2009) 927–936.
[8] C.E. Hayes, W.A. Edelstein, J.F. Schenck, O.M. Mueller, M. Eash, An efficient, highly homogeneous radiofrequency coil for whole-body NMR imaging at 1.5-T, J. Magn. Reson. 63 (1985) 622–628.
[9] J.T. Vaughan, H.P. Hetherington, J.O. Otu, J.W. Pan, G.M. Pohost, High frequency volume coils for clinical NMR imaging and spectroscopy, Magn. Reson. Med. 32 (1994) 206–218.
[10] D. Sullivan, Mathematical-methods for treatment planning in deep regional hyperthermia, IEEE Trans. Microwave Theory Tech. 39 (1991) 864–872.
[11] P. Wust, J. Nadobny, R. Felix, P. Deuflhard, A. Louis, W. John, Strategies for optimized application of annular-phased-array systems in clinical hyperthermia, Int. J. Hyperthermia 7 (1991) 157–173.
[12] M. Weihrauch, P. Wust, M. Weiser, J. Nadobny, S. Eisenhardt, V. Budach, J. Gellermann, Adaptation of antenna profiles for control of MR guided hyperthermia (HT) in a hybrid MR-HT system, Med. Phys. 34 (2007) 4717–4725.
[13] M.E. Kowalski, H.M. Jin, Model-based optimization of phased arrays for electromagnetic hyperthermia, IEEE Trans. Microwave Theory Tech. 52 (2004) 1964–1977.
[14] G. Adriany, P.F. van de Moortele, F. Wiesinger, S. Moeller, J.P. Strupp, P. Andersen, C. Snyder, X. Zhang, W. Chen, K.P. Pruessmann, P. Boesiger, T. Vaughan, K. Ugurbil, Transmit and receive transmission line arrays for 7 Tesla parallel imaging, Magn. Reson. Med. 53 (2005) 434–445.
[15] G. Adriany, P.F. van de Moortele, J. Ritter, S. Moeller, E.J. Auerbach, C. Akgun, C.J. Snyder, T. Vaughan, K. Ugurbil, A geometrically adjustable 16-channel transmit/receive transmission line array for improved RF efficiency and parallel imaging performance at 7 Tesla, Magn. Reson. Med. 59 (2008) 590–597.
[16] G.J. Metzger, C. Snyder, C. Akgun, T. Vaughan, K. Ugurbil, P.F. van de Moortele, Local B_1^+ shimming for prostate imaging with transceiver arrays at 7 T based on subject-dependent transmit phase measurements, Magn. Reson. Med. 59 (2008) 396–409.
[17] K.N. Kurpad, S.M. Wright, E.B. Boskamp, RF current element design for independent control of current amplitude and phase in transmit phased arrays, Conc. Magn. Reson. B 29B (2006) 75–83.
[18] O. Kraff, A.K. Bitz, S. Kruszona, S. Orzada, L.C. Schaefer, J.M. Theysohn, S. Maderwald, M.E. Ladd, H.H. Quick, An eight-channel phased array RF coil for spine MR imaging at 7 T, Invest. Radiol. 44 (2009) 734–740.
[19] S. Saekho, F.E. Boada, D.C. Noll, V.A. Stenger, Small tip angle three-dimensional tailored radiofrequency slab-select pulse for reduced B_1 inhomogeneity at 3 T, Magn. Reson. Med. 53 (2005) 479–484.
[20] S. Saekho, C.Y. Yip, D.C. Noll, F.E. Boada, V.A. Stenger, Fast-kz three-dimensional tailored radiofrequency pulse for reduced B_1 inhomogeneity, Magn. Reson. Med. 55 (2006) 719–724.
[21] C.M. Collins, Z.W. Wang, W.H. Mao, J.M. Fang, W.Z. Liu, M.B. Smith, Array-optimized composite pulse for excellent whole-brain homogeneity in high-field MRI, Magn. Reson. Med. 57 (2007) 470–474.
[22] K. Setsompop, V. Alagappan, B. Gagoski, T. Witzel, J. Polimeni, A. Potthast, F. Hebrank, U. Fontius, F. Schmitt, L.L. Wald, E. Adalsteinsson, Slice-selective RF pulses for in vivo B_1^+ inhomogeneity mitigation at 7 Tesla using parallel RF excitation with a 16-element coil, Magn. Reson. Med. 60 (2008) 1422–1432.
[23] K. Setsompop, L.L. Wald, V. Alagappan, B.A. Gagoski, E. Adalsteinsson, Magnitude least squares optimization for parallel radio frequency excitation design demonstrated at 7 Tesla with eight channels, Magn. Reson. Med. 59 (2008) 908–915.
[24] K. Setsompop, V. Alagappan, B.A. Gagoski, A. Potthast, F. Hebrank, U. Fontius, F. Schmitt, L.L. Wald, E. Adalsteinsson, Broadband slab selection with B_1^+ mitigation at 7 T via parallel spectral–spatial excitation, Magn. Reson. Med. 61 (2009) 493–500.
[25] A.C. Zelinski, L.L. Wald, K. Setsompop, V. Alagappan, B.A. Gagoski, V.K. Goyal, E. Adalsteinsson, Fast slice-selective radio-frequency excitation pulses for mitigating B_1^+ inhomogeneity in the human brain at 7 Tesla, Magn. Reson. Med. 59 (2008) 1355–1364.
[26] Q.X. Yang, W. Mao, J. Wang, M.B. Smith, H. Lei, X. Zhang, K. Ugurbil, W. Chen, Manipulation of image intensity distribution at 7.0 T: passive RF shimming and focusing with dielectric materials, J. Magn. Reson. Imaging 24 (2006) 197–202.
[27] A. Sreenivas, M. Lowry, P. Gibbs, M. Pickles, L.W. Turnbull, A simple solution for reducing artefacts due to conductive and dielectric effects in clinical magnetic resonance imaging at 3 T, Eur. J. Radiol. 62 (2007) 143–146.
[28] Y. Takayama, H. Nonaka, M. Nakajima, T. Obata, H. Ikehira, Reduction of a high-field dielectric artifact with homemade gel, Magn. Reson. Med. Sci. 7 (2008) 37–41.
[29] T. Sunaga, H. Ikehira, S. Furukawa, M. Tamura, E. Yoshitome, T. Obata, H. Shinkai, S. Tanada, H. Murata, Y. Sasaki, Development of a dielectric equivalent gel for better impedance matching for human skin, Bioelectromagnetics 24 (2003) 214–217.
[30] K. Haines, T. Neuberger, M. Lanagan, E. Semouchkina, A.G. Webb, High Q calcium titanate cylindrical dielectric resonators for magnetic resonance microimaging, J. Magn. Reson. 200 (2009) 349–353.
[31] T. Neuberger, V. Tyagi, E. Semouchkina, M. Lanagan, A. Baker, K. Haines, A.G. Webb, Design of a ceramic dielectric resonator for NMR microimaging at 14.1 Tesla, Concepts Magn. Reson. B Magn. Reson. Eng. 33B (2008) 109–114.
[32] T.Q. Li, G.P. van, H. Merkle, L. Talagala, A.P. Koretsky, J. Duyn, Extensive heterogeneity in white matter intensity in high-resolution T_2^*-weighted MRI of the human brain at 7.0 T, Neuroimage 32 (2006) 1032–1040.
[33] T. Horiuchi, M. Takahashi, J. Kikuchi, S. Yokoyama, H. Maeda, Effect of dielectric properties of solvents on the quality factor for a beyond 900 MHz cryogenic probe model, J. Magn. Reson. 174 (2005) 34–42.
[34] A. Sihvola, Mixing rules with complex dielectric coefficients, Subsurf. Sensing Technol. Appl. 1 (2000) 393–415.
[35] K. Kollia, S. Maderwald, N. Putzki, M. Schlamann, J.M. Theysohn, O. Kraff, M.E. Ladd, M. Forsting, I. Wanke, First clinical study on ultra-high-field MR imaging in patients with multiple sclerosis: comparison of 1.5 T and 7 T, AJNR Am. J. Neuroradiol. 30 (2009) 699–702.
[36] K.E. Hammond, M. Metcalf, L. Carvajal, D.T. Okuda, R. Srinivasan, D. Vigneron, S.J. Nelson, D. Pelletier, Quantitative in vivo magnetic resonance imaging of multiple sclerosis at 7 Tesla with sensitivity to iron, Ann. Neurol. 64 (2008) 707–713.
[37] J.H. Duyn, G.P. van, T.Q. Li, J.A. de Zwart, A.P. Koretsky, M. Fukunaga, High-field MRI of brain cortical substructure based on signal phase, Proc. Natl. Acad. Sci. USA 104 (2007) 11796–11801.